Electron-Scale Reconnecting Current Sheet Formed Within the Lower-Hybrid Wave-Active Region of Kelvin-Helmholtz Waves

Blasl, K. A.; Nakamura, T. K.M.; Nakamura, R.; Settino, A.; Hasegawa, H.; Vörös, Z.; Hosner, M.; Schmid, D.; Volwerk, M.; Roberts, Owen W.; Panov, E.; Liu, Yi Hsin; Plaschke, F.; Stawarz, J. E.; Holmes, J. C.

Published in:
Geophysical Research Letters

DOI:
10.1029/2023GL104309
10.5281/zenodo.7869234
10.5281/zenodo.7875822
10.5281/zenodo.8217728

Publication date:
2023

Citation for published version (APA):
Blasl, K. A., Nakamura, T. K. M., Nakamura, R., Settino, A., Hasegawa, H., Vörös, Z., Hosner, M., Schmid, D., Volwerk, M., Roberts, O. W., Panov, E., Liu, Y. H., Plaschke, F., Stawarz, J. E., & Holmes, J. C. (2023). Electron-Scale Reconnecting Current Sheet Formed Within the Lower-Hybrid Wave-Active Region of Kelvin-Helmholtz Waves. *Geophysical Research Letters*, *50*(19), Article e2023GL104309. https://doi.org/10.1029/2023GL104309, https://doi.org/10.5281/zenodo.7869234, https://doi.org/10.5281/zenodo.7875822, https://doi.org/10.5281/zenodo.8217728

Geophysical Research Letters

Supporting Information for

Electron-scale reconnecting current sheet formed within the lower hybrid wave-active region of Kelvin-Helmholtz waves

K. A. Blasl[1,2], T. K. M. Nakamura[1,9], R. Nakamura[1], A. Settino[1], H. Hasegawa[3], Z. Vörös[1,4], M. Hosner[1,2], D. Schmid[1], M. Volwerk[1], Owen W. Roberts[1], E. Panov[1], Yi-Hsin Liu[5], F. Plaschke[6], J. E. Stawarz[7], J. C. Holmes[8]

[1] Space Research Institute, Austrian Academy of Sciences, 8042 Graz, Styria, Austria
[2] Universität Graz, Institut für Physik, Universitätsplatz 5, 8010 Graz, Styria, Austria
[3] Institute of Space and Astronautical Science, Japan Aerospace Exploration Agency, Sagamihara, Kanagawa 252-5210, Japan
[4] Institute of Earth Physics and Space Science, ELRN, 9400 Sopron, Hungary
[5] Department of Physics and Astronomy, Dartmouth College, Hanover, New Hampshire 03755, USA
[6] Institut für Geophysik und extraterrestrische Physik, TU Braunschweig, 38106 Braunschweig, Germany
[7] Department of Physics, Imperial College London, London SW7 2AZ, UK
[8] Los Alamos National Laboratory, Los Alamos, New Mexico 87545, USA
[9] Krimgen LLC, Hiroshima 739-1731, Japan

Contents of this file

Introduction

This supporting information provides the data sets used for the analysis in the manuscript in Text S1. In Text S2 we provide the details on the simulation setup and the normalizations used in Fig. 4 of the main text. In Figure S1, we show the 3D formation plot of the four MMS spacecraft on September 23, 2017, around 16:07:30 UTC in the local LMN coordinate system used in the main text. Figure S2 shows the temporal evolution of the normalized reconnection rate for the X-line shown in Figure 3 of the main text. It was calculated as the time difference of the vector potential at the X-line. We indicate the three time steps shown in Figure 3 of the main text by the three vertical dashed lines in Figure S2. Figure S3 shows results from the Minimum Directional Derivative (MDD) method by Shi et al. (2019) used to study the dimensionality of the current sheet in more detail to distinguish between the influence of spatial and temporal variations in the data. Finally, Figure S4 shows results from the Polynomial

Reconstruction method (Denton et al., 2020; Hosner et al., 2022) applied to this current sheet event between 16:07:19.331 UT and 16:07:19.6 UT.

Text S1.

Data sets: This study analyses data from MMS (Burch et al., 2016). Fluxgate Magnetometers (FGMs) (Russell et al., 2016) provide the magnetic field data in fast and burst survey modes, at 16 and 128 Hz, respectively. The electric field data are provided by the Electric Field Double Probes (EDPs) (Ergun et al., 2016; Lindqvist et al., 2016), in fast and burst modes, at 32 and 8192 Hz, respectively. Particle moments for ions (electrons) are employed from the Fast Plasma Investigation (FPI) (Pollock et al., 2016) instruments in burst mode at a cadence of 150 (30) ms and in fast mode at 4.5 s.

As in our previous study (Blasl et al., 2022), to analyze the large-scale KH waves/vortices we employ a global boundary normal (x′, y′, z′) coordinate system, which has been introduced by Russell and Elphic (1978). The normal axis y′ is chosen in the outward direction perpendicular to a modelled magnetopause boundary (Shue et al., 1997). x′ is the cross-product between y′ and the Geocentric Solar Magnetic (GSM) z-axis which approximately corresponds to the direction opposing the magnetosheath flow along the magnetopause dusk flank. Finally, z′ approximately corresponds to the Solar North direction of the Geocentric Solar Ecliptic (GSE) system (z_{GSE}) and completes the right-hand orthogonal system. The new directions, illustrated in Fig. 1g of the main text, have the GSE coordinates of z′ = (0.00,−0.29, 0.96), x′ = (0.96,−0.28, 0.09) and y′ = (0.29, 0.91, 0.28). To create the wave power plots of the electric field shown in Fig. 1f we employed the *wavpol.pro* routine of SPEDAS. For the data in panels (j)-(m) of Fig. 2, we used local LMN coordinates obtained from the Minimum Variance Analysis (MVA) (Sonnerup & Cahill, 1967) to analyze the electron-scale current sheet as explained in Sec. 2.2 of the main text.

Text S2.

Simulation details: The 2.5D PIC simulation employed in this paper modelling the observed current sheet event shown in Fig. 2 was set up with a realistic ion-to-electron mass ratio of $m_i/m_e = 1836$. The ratio of the electron plasma frequency and the electron gyrofrequency was set to $\omega_{p,e}/\omega_{c,e} = 4.0$. The coordinates in the simulation (Fig. 3 of main text) correspond to a local co-rotating LMN system labelled (L′, M, N′) different from the static LMN system derived from MMS data (cf. Fig. 3 of main text and Fig. S4 of Supporting Information). The virtual spacecraft path shown in Fig. 3 follows the LMN system shown in Fig. S4 and the virtual data in Fig. 4 of the main text. The system size of this run was set to (L_x x L_y = 4 d_i x 2 d_i = 2304 x 1152) cells with a total of approximately $2 \cdot 10^{10}$ super-particles. Note that in Fig. 3 we show a zoomed-in view near an X-line. The initial current sheet thickness was set to $\Delta \approx 2\ d_e$ and the initial current is carried only by electrons. Due to the weak density jump and velocity shear observed across the current sheet, we employed a uniform density in the simulation with no velocity shear between the two sides. The magnetic field was set up as $B = B_o \cdot \tanh(N/\Delta) + B_g$, with $B_o = 2$ nT. Further, we employed a uniform guide field with a guide field to reconnecting field ratio of $B_g / B_o = 5.0$, following the MMS observations. The electron temperature is set to be higher in the current sheet than in the background plasma in order to sustain the pressure balance, while the ion temperature is set to be uniform with the ion-to-electron temperature ratio at the current sheet center of $T_i / T_e = 12.0$.

Normalizations: For a point-to-point comparison of MMS observations and simulation results in Fig. 4, we normalize the data as follows: the magnetic field data are normalized to the reconnecting component B_0 = 2 nT, velocity data to the ion Alfvén velocity $v_{A,i}$ = 56 km/s (calculated from B_0 and the density on the magnetospheric side n_0 = 0.6 cm^{-3}), electric field data to ($v_{A,i}$ B_0) and the energy conversion parameter $J \cdot E'$ (Zenitani et al., 2011) to ($v_{A,i}$ B_0^2/d_i), where d_i was calculated from n_0. The simulation data of $v_{e,N}$ and E_N have additionally been smoothed using the moving average method (box size of 15) to highlight the general trend of the data.

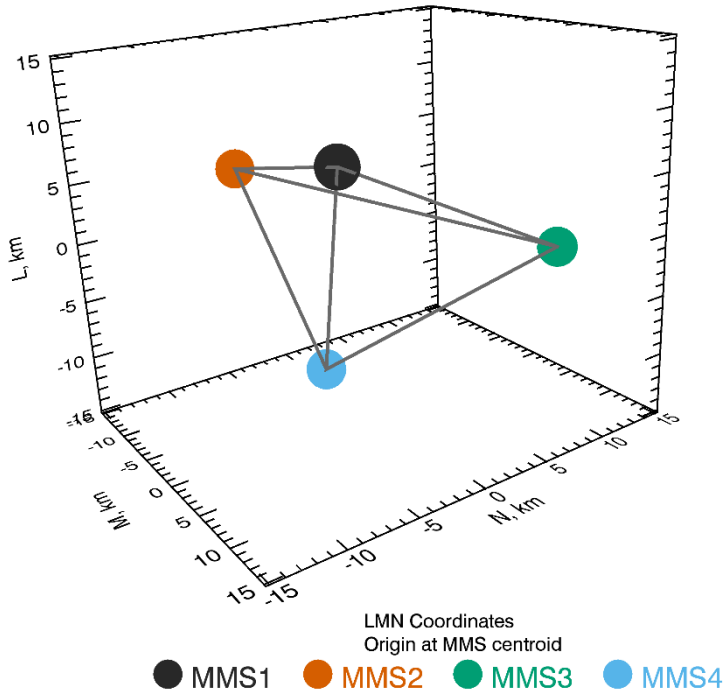

Figure S1. MMS spacecraft formation plot on September 23, 2017, around 16:07:30 UTC in the local LMN coordinate system.

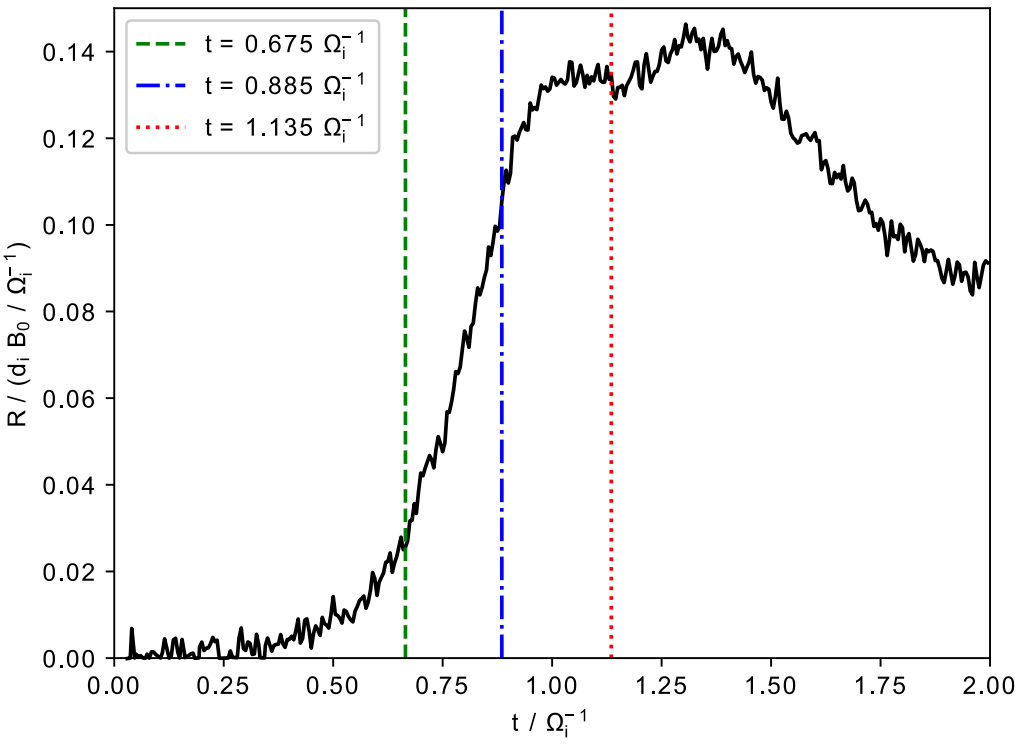

Figure S2. Temporal evolution of the normalized reconnection rate for the X-line in the simulation shown in Fig. 3. The three vertical lines indicate the three time steps shown in Fig. 3.

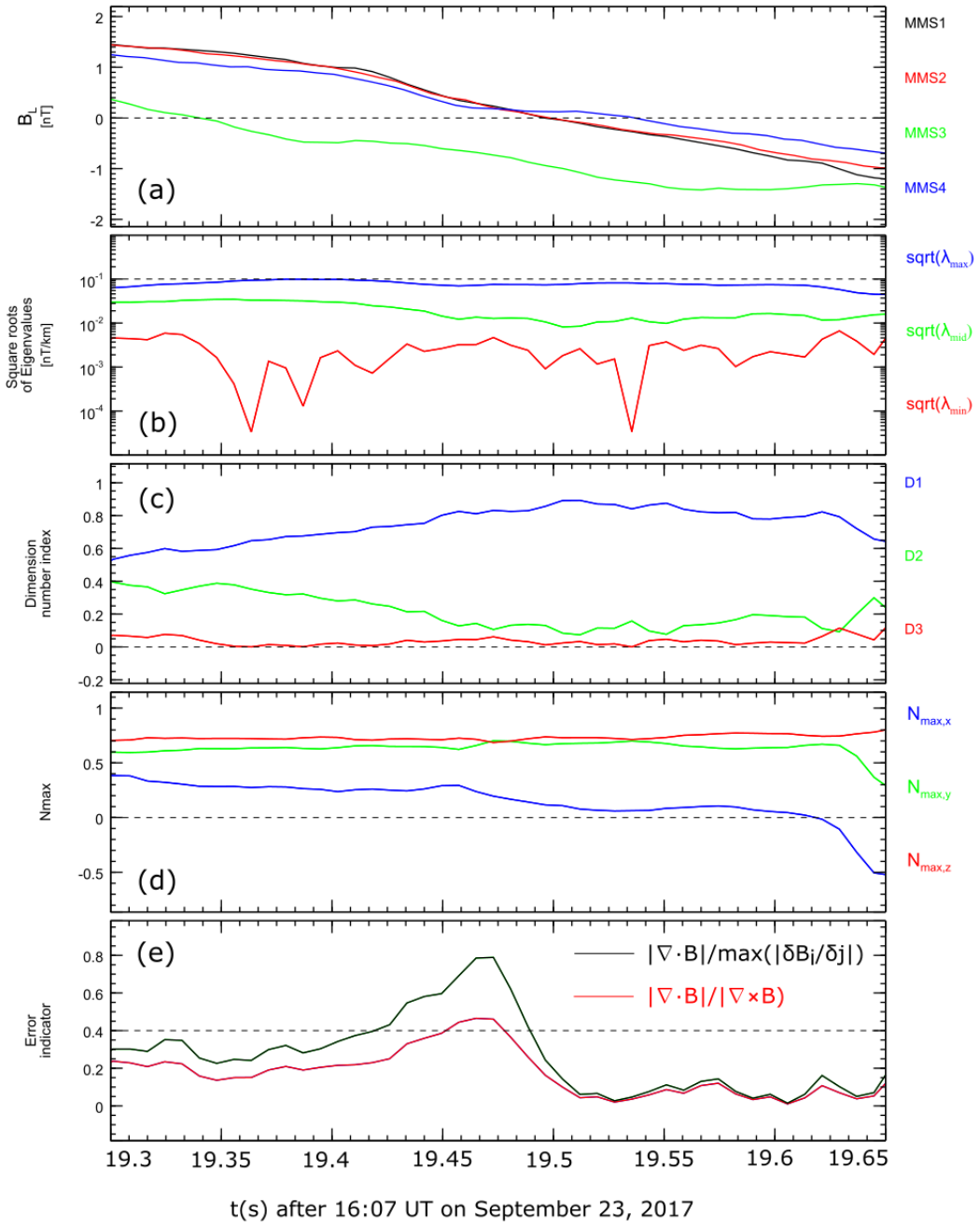

Figure S3. Results from the Minimum Directional Derivative (MDD) method (Shi et al., 2019) for the current sheet crossing shown in Fig. 2 (j)-(m) in the main text between 16:07:19.3 UT and 16:07:19.65 UT on September 23, 2017. (a) Reconnecting magnetic field component B_L. (b) Square roots of the maximum, intermediate and minimum eigenvalues (λ_{max}, λ_{mid}, λ_{min}) of the 3x3 MDD matrix (Shi et al., 2019). (c) Measures of the dimensionality of the structure encountered by the spacecraft (Rezeau et al., 2018), defined as $D1 = (\lambda_{max} - \lambda_{mid})/\lambda_{max}$, $D2 = (\lambda_{mid} - \lambda_{min})/\lambda_{max}$ and $D3 = \lambda_{min}/\lambda_{max}$. (d) GSE components of the eigenvector corresponding to the maximum eigenvalue (i.e., the normal direction). (e) Error indicators defined as $|\nabla \cdot \mathbf{B}|/\max(|\delta B_i/\delta j|)$ and $|\nabla \cdot \mathbf{B}|/|\nabla \times \mathbf{B}|$.

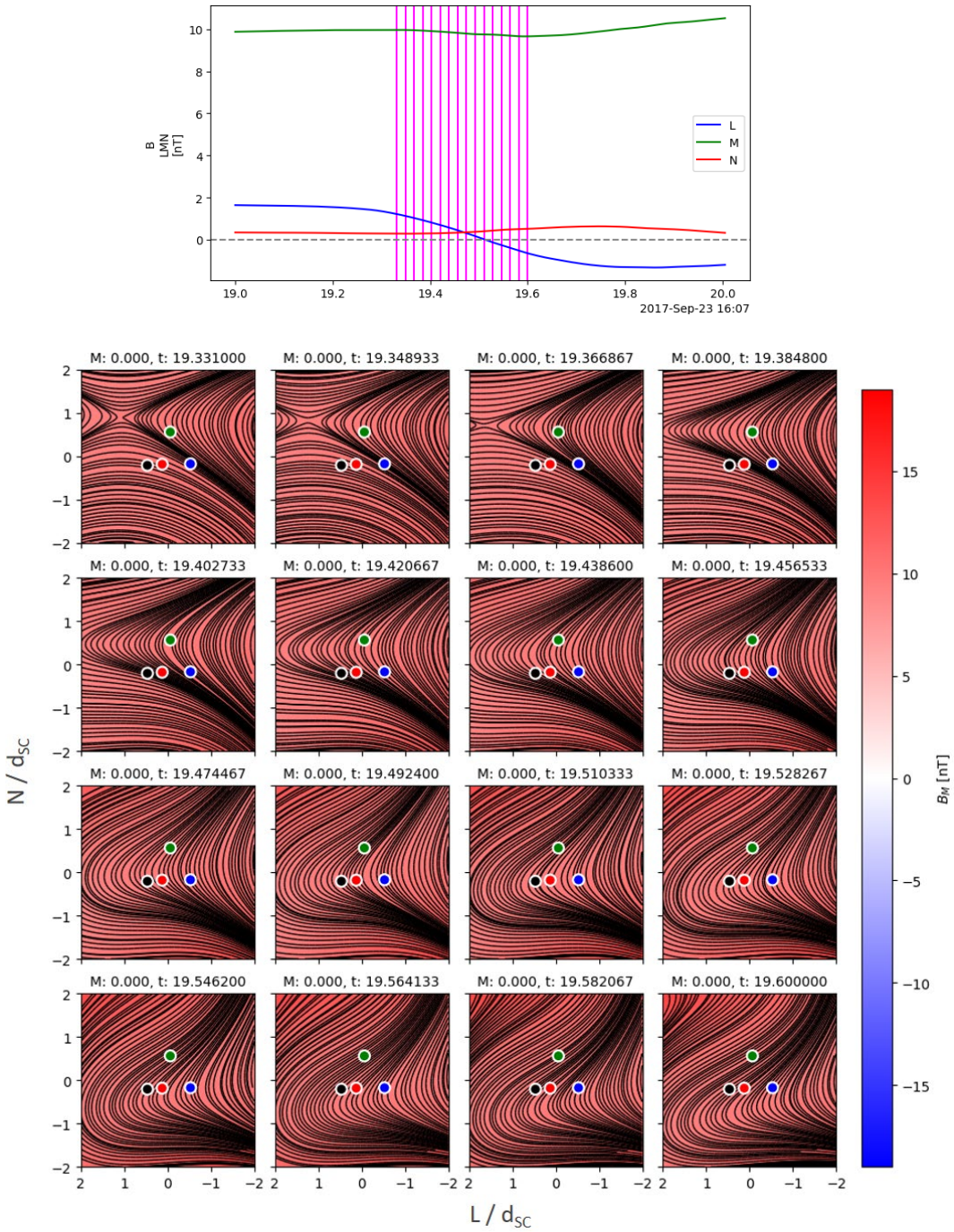

Figure S4. Results from the 3D reduced quadratic model of the Polynomial Reconstruction method (Denton et al., 2020; Hosner et al., 2022) applied to the current sheet event between 16:07:19.331 UT and 16:07:19.6 UT. The top figure shows the magnetic field in the local LMN coordinate system between 16:07:19 UT and 16:07:20 UT. The vertical magenta lines indicate the time slices used to display the Reconstruction results depicted below. The results are shown in the L-N plane of the local LMN coordinate system and the axes are labeled in multiples of the average spacecraft separation of $d_{SC} \approx 20.2$km. The color code shows the out-of-plane magnetic field. MMS color code: MMS1=black, MMS2=red, MMS3=green, MMS4=blue